ARTICLE

www.the-innovation.org

Antagonism between ambient ozone increase and urbanization-oriented population migration on Chinese cardiopulmonary mortality

Haitong Zhe Sun,[1,2,3,19] Junchao Zhao,[4,19] Xiang Liu,[5] Minghao Qiu,[6] Huizhong Shen,[7] Serge Guillas,[8,9] Chiara Giorio,[1] Zosia Staniaszek,[1] Pei Yu,[10] Michelle W.L. Wan,[1] Man Mei Chim,[1] Kim Robin van Daalen,[11,12,13] Yilin Li,[1] Zhenze Liu,[14] Mingtao Xia,[15] Shengxian Ke,[16] Haifan Zhao,[17] Haikun Wang,[5] Kebin He,[4] Huan Liu,[4,*] Yuming Guo,[10,*] and Alexander T. Archibald[1,18,*]

*Correspondence: liu_env@tsinghua.edu.cn (H.L.); yuming.guo@monash.edu (Y.G.); ata27@cam.ac.uk (A.T.A.)

Received: June 26, 2023; Accepted: September 17, 2023; Published Online: September 20, 2023; https://doi.org/10.1016/j.xinn.2023.100517

GRAPHICAL ABSTRACT

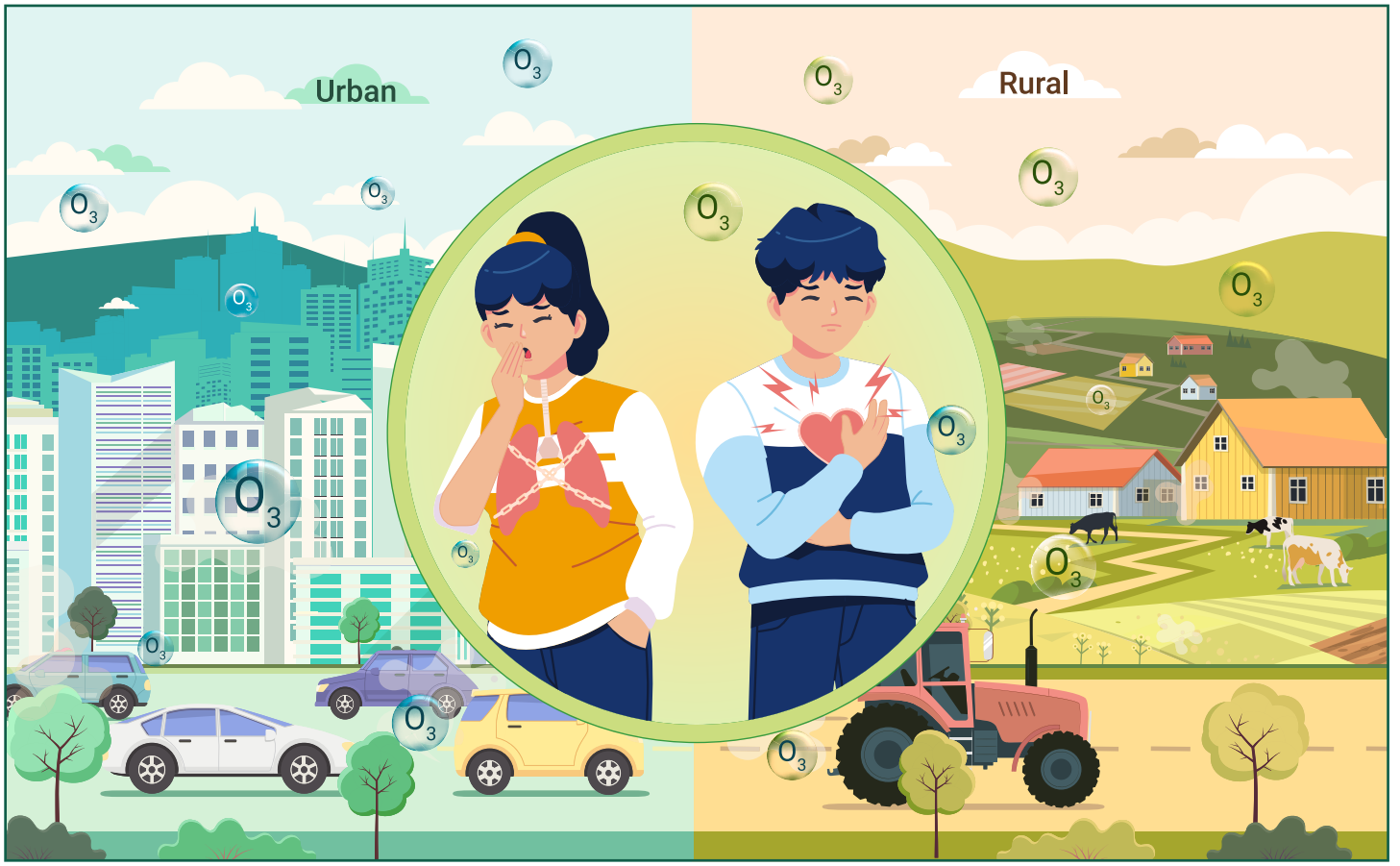

PUBLIC SUMMARY

- Rural O_3 exposure is ~10 ppb higher than that of adjacent urban areas in China.
- Excess cardiopulmonary deaths rise from 299,500 in 1990 to 373,500 in 2019.
- Premature cardiovascular deaths due to long-term O_3 exposure are overlooked.
- Urban migration reduces population-weighted O_3 exposure and associated mortality.

ARTICLE

Antagonism between ambient ozone increase and urbanization-oriented population migration on Chinese cardiopulmonary mortality

Haitong Zhe Sun,[1,2,3,19] Junchao Zhao,[4,19] Xiang Liu,[5] Minghao Qiu,[6] Huizhong Shen,[7] Serge Guillas,[8,9] Chiara Giorio,[1] Zosia Staniaszek,[1] Pei Yu,[10] Michelle W.L. Wan,[1] Man Mei Chim,[1] Kim Robin van Daalen,[11,12,13] Yilin Li,[1] Zhenze Liu,[14] Mingtao Xia,[15] Shengxian Ke,[16] Haifan Zhao,[17] Haikun Wang,[5] Kebin He,[4] Huan Liu,[4,*] Yuming Guo,[10,*] and Alexander T. Archibald[1,18,*]

[1]Yusuf Hamied Department of Chemistry, University of Cambridge, Cambridge CB2 1EW, UK

[2]Department of Earth Sciences, University of Cambridge, Cambridge CB2 3EQ, UK

[3]Department of Environmental Health and Engineering, Johns Hopkins Bloomberg School of Public Health, Baltimore, MD 21205, USA

[4]State Key Joint Laboratory of ESPC, State Environmental Protection Key Laboratory of Sources and Control of Air Pollution Complex, School of Environment, Tsinghua University, Beijing 100084, China

[5]School of Atmospheric Sciences, Nanjing University, Nanjing 210023, China

[6]Department of Earth System Science, Stanford University, Stanford, CA 94305, USA

[7]School of Environmental Science and Engineering, Southern University of Science and Technology, Shenzhen 518055, China

[8]Department of Statistical Science, University College London, London WC1E 6BT, UK

[9]The Alan Turing Institute, London NW1 2DB, UK

[10]School of Public Health and Preventive Medicine, Monash University, Melbourne, VIC 3004, Australia

[11]British Heart Foundation Cardiovascular Epidemiology Unit, Department of Public Health and Primary Care, University of Cambridge, Cambridge CB1 8RN, UK

[12]Heart and Lung Research Institute, University of Cambridge, Cambridge CB2 0BD, UK

[13]Barcelona Supercomputing Center, Department of Earth Sciences, 08034 Barcelona, Spain

[14]School of Environmental Science and Engineering, Nanjing University of Information Science and Technology, Nanjing 210044, China

[15]Department of Mathematics, University of California, Los Angeles, Los Angeles, CA 90095, USA

[16]State Key Laboratory of New Ceramics and Fine Processing, Key Laboratory of Advanced Materials of Ministry of Education, School of Materials Science and Engineering, Tsinghua University, Beijing 100084, China

[17]Department of Engineering, University of Cambridge, Cambridge CB2 1PZ, UK

[18]National Centre for Atmospheric Science, Cambridge CB2 1EW, UK

[19]These authors contributed equally

*Correspondence: liu_env@tsinghua.edu.cn (H.L.); yuming.guo@monash.edu (Y.G.); ata27@cam.ac.uk (A.T.A.)

Received: June 26, 2023; Accepted: September 17, 2023; Published Online: September 20, 2023; https://doi.org/10.1016/j.xinn.2023.100517

Citation: Sun H.Z., Zhao J., Liu X., et al., (2023). Antagonism between ambient ozone increase and urbanization-oriented population migration on Chinese cardiopulmonary mortality. The Innovation **4(6)**, 100517.

Ever-increasing ambient ozone (O_3) pollution in China has been exacerbating cardiopulmonary premature deaths. However, the urban-rural exposure inequity has seldom been explored. Here, we assess population-scale O_3 exposure and mortality burdens between 1990 and 2019 based on integrated pollution tracking and epidemiological evidence. We find Chinese population have been suffering from climbing O_3 exposure by 4.3 ± 2.8 ppb per decade as a result of rapid urbanization and growing prosperity of socioeconomic activities. Rural residents are broadly exposed to 9.8 ± 4.1 ppb higher ambient O_3 than the adjacent urban citizens, and thus urbanization-oriented migration compromises the exposure-associated mortality on total population. Cardiopulmonary excess premature deaths attributable to long-term O_3 exposure, 373,500 (95% uncertainty interval [UI]: 240,600–510,900) in 2019, is underestimated in previous studies due to ignorance of cardiovascular causes. Future O_3 pollution policy should focus more on rural population who are facing an aggravating threat of mortality risks to ameliorate environmental health injustice.

INTRODUCTION

Photochemical smog events of Los Angeles in the 1940s aroused public awareness to surface ozone (O_3) pollution for the first time. As a secondary air pollutant, O_3 is formed from a collection of precursor chemicals including NO_X (NO_2 and NO), carbon monoxide, and volatile organic compounds (VOCs), through complex photochemical reactions and NO_X-RO_X (RO and RO_2) cycles.[1] Anthropogenic emissions from vehicles, petrochemical industries, coal-fired power plants, and other types of incomplete combustions exacerbate the O_3 pollution.[2,3] While deforestation decreases biogenic activities, global warming enhances biogenic emissions of VOCs (e.g., isoprene), which also adds on to the surface O_3 burden.[4] High ambient O_3 pollution has been causing significant population health issues. Epidemiological studies show that short-term high-concentration exposure to ambient O_3 can cause asthma exacerbation,[5] respiratory symptoms,[6] myocardial infarction,[7] or even cardiac arrest,[8] and long-term O_3 exposure can even increase the mortality risks of chronic respiratory diseases (CRDs) and cardiovascular diseases (CVDs).[9] Hence, understanding the spatiotemporal pattern of ambient O_3 will be of incontrovertible significance for public health protection.

The TOAR (Tropospheric Ozone Assessment Report) collaborative network[10] and CNEMC (China National Environmental Monitoring Center)[11] have been archiving *in situ* ambient O_3 observations, but the selective spatial representativeness will hamper the credibility of exposure assessment for populations residing distant from monitoring sites. Chemical reanalysis[12] and satellite-based remote-sensing measurements[13] have been playing an irreplaceable role in ambient O_3 tracking. Besides the conventional chemical transport models (CTMs),[14] the state-of-the-art coupled Earth system models with interactive chemistry-climate feedback collated by CMIP6 (Coupled Model Intercomparison Project Phase 6) provide long-timescale full coverage global ambient O_3 numerical simulation ensemble.[15] The booming of artificial intelligence algorithms makes it feasible to fuse these seamless products and the scattered observations, yielding high-quality fused databases.[16-20] Due to the rapid photochemical and radical-involved kinetic reactions, ambient O_3 is of high geographical variability. Rural environments are observed to be of higher ambient O_3 pollution,[21,22] a key point omitted in many large-scale population health impact assessment studies, and thus the urban-rural environmental injustice has long been overlooked. We herein synthesize multiple well-developed ambient O_3 concentration databases with urban-rural differentiation to better characterize the population exposure levels restricting biases or errors from any single sources.

Previous O_3-mortality estimation studies only considered premature deaths caused by chronic obstructive pulmonary disease (COPD) due to the limited epidemiological evidence.[23] We accomplish a systematic review to collect up-to-date O_3-mortality associations from cohort studies on long-term O_3 exposure-associated multi-cause mortality, and conduct meta-analysis to pool the estimated exposure-response association strengths (i.e., relative risks).[9] With the help of the China Statistical Yearbook series, we calibrated the Chinese population, and then linked the ambient O_3 exposure and exposure-response relationships to estimate the excess mortalities among Chinese population during 1990–2019. Cohort-based relative risks are estimated using Cox regression, assuming relative hazard keeps constant along with the time series. Therefore, cross-sectional urban-rural distinguished populations are sufficient for mortality

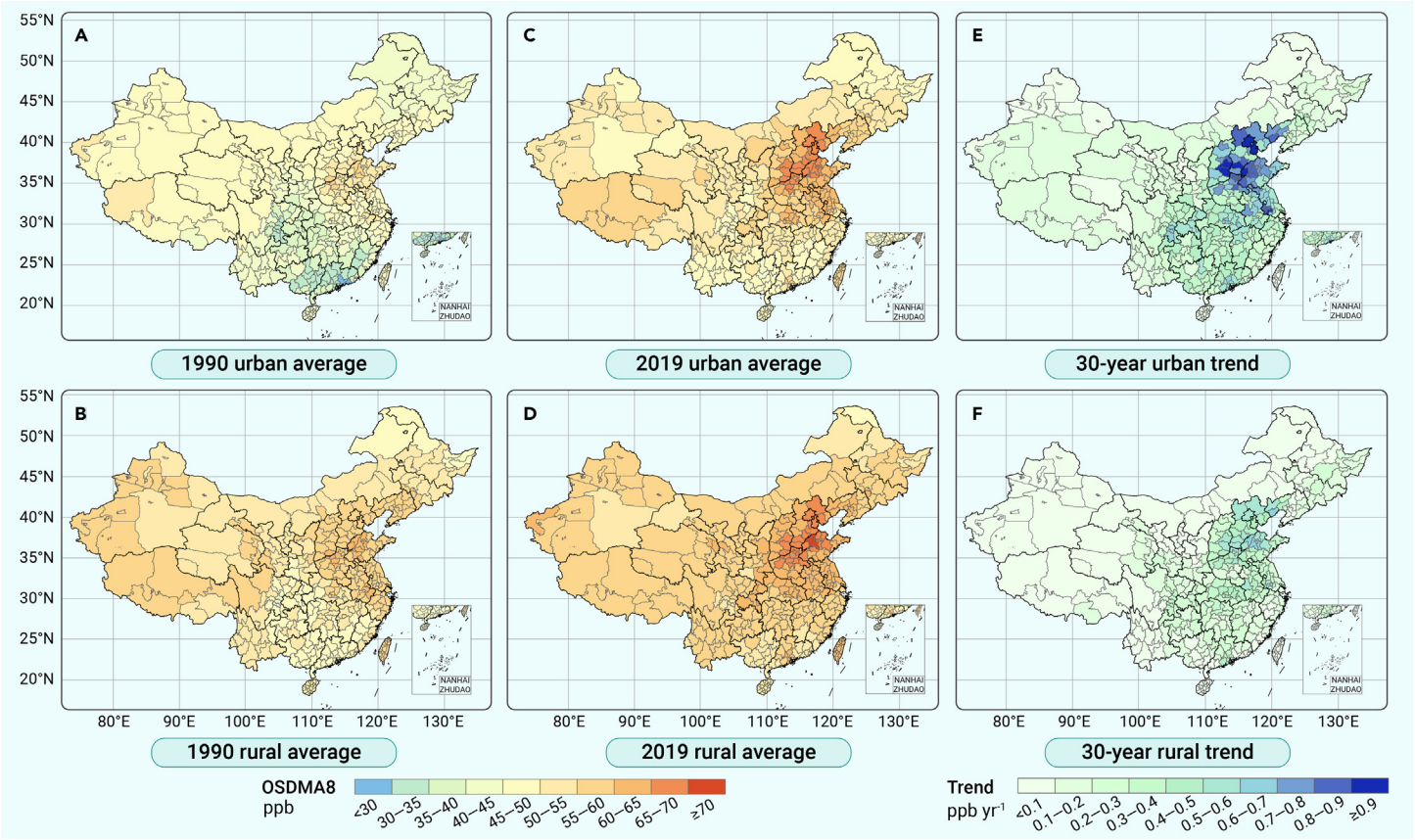

Figure 1. Mapping of prefecture-city-level ambient ozone and temporal trends (A and B) Peak ambient ozone concentrations with urban-rural differentiation for 1990 by metric of 6-month (April to September) ozone-season daily 8-h maximum average (OSDMA8, ppb). (C and D) Peak ambient ozone concentrations for 2019 by OSDMA8. (E and F) Thirty-year annual average change rates. Upper panels (A, C, and E) are distinguished for urban residential environments, and lower panels (B, D, and F) for rural living environments. Ambient ozone concentrations in 10-km spatial resolution are predicted by fusion of multiple downscaled data products (see Methods S1 and S2) and are averaged for mapping in prefecture-level cities. Urban and rural temporal change rates for each prefectural city are estimated by generalized linear model. Province-level statistics for 1990 and 2019 are listed in Table S1. Base-map of China credits to Ministry of Natural Resources, PRC.

estimation, and there is no need to consider accumulative exposure or individual-level rural-to-urban migration history.

Throughout this study, we aim to underscore the urban-rural disparity of ambient O_3 pollution across China, and emphasize the severity of cardiopulmonary mortalities attributable to O_3 exposure. Urbanization refers to the phenomenon that the originally low-population density settlements become a city due to the gradual gathering of population and frequentialized economic activities, leading to a social structure change that rural population are gradually transformed into urban residents. We thus define rural-to-urban migration and rural residents whose habitations are urbanized both as urbanization-oriented population migration to distinguish the urban and rural residents, as reflected in the cross-sectional population density offered by United Nations World Population Prospects.[24] Rural residents contribute much lower anthropogenic emissions of O_3 precursors (especially NO_X by vehicles) than urban citizens, but are unfairly exposed to higher O_3 pollution. Those moving to cities can reduce their exposure level, while there is always a certain proportion of rural residents (e.g., living relying on farming) lacking willingness or capability to migrate. In this sense, we underline the higher rural O_3 exposure, and highlight the antagonism effect between the gradually increasing ambient O_3 concentrations and the population migration to assist in understanding the dynamics of total O_3 exposure-associated excess mortality. We intend to inform the policymakers to be aware of the urban-rural environmental justice in terms of ambient O_3 exposure, echoing the Sustainable Development Goals advocated by the United Nations (e.g., SDG 3) to ensure healthy lives and promote well-being for the whole population.

RESULTS

Spatiotemporal patterns of urban-rural differentiated ambient ozone

We fuse four well-established data products calibrated by *in situ* observations (see Methods S1 and S2) to quantify the urban and rural population exposure to ambient O_3 scaled in 6 months (April to September) using the ozone-season daily 8-h maximum average (OSDMA8) metric (see geographical mapping of starting year 1990 and endpoint year 2019 aggregated by prefecture-level cities in Figures 1A–1D, and province-level statistics in Table S1). Rural O_3 pollution was generally more severe, as 9.8 ± 4.1 ppb higher than the adjacent urban O_3 concentrations, averaging over 30 studied years.

Higher O_3 pollution mainly clustered in Jing-Jin-Ji and adjacent areas (i.e., Shanxi, Henan, Shandong, Anhui, and Jiangsu Province), where the highest climbing rates concurrently occurred (Figures 1E and 1F). In 1990, the nationwide ambient O_3 exposure was 40.4 ± 8.1 ppb for all urban citizens, and 54.0 ± 5.7 ppb for rural residents. In 2019, rural O_3 rose to 67.6 ± 10.2 ppb by an increasing rate of around 3.9 ± 2.7 ppb per decade, and urban O_3 climbed to 59.2 ± 12.6 ppb by a more prominent increasing speed of approximately 6.2 ± 3.4 ppb per decade.

We present the country-level and region-specific (seven administrative geographical divisions and four megalopolises, see definitions in Methods S3 and Figure S1) longitudinal trends of urban, rural, and population-weighted exposure (PWE) to ambient O_3 in Figure S2. Among the seven geographical divisions, the highest O_3 pollution exacerbation rates were observed in East China (7.6 ppb per decade), followed by South (6.1 ppb per decade) and Central China (5.9 ppb per decade). Four megalopolises suffered rapid deterioration, especially the Jing-Jin-Ji urban agglomeration (9.2 ppb per decade). The lowest population O_3 exposure increases occurred in Northwest China (2.3 ppb per decade). PWE also reflects the relative proportions of urban-rural residents in the studied areas, that in less-urbanized regions (e.g., Northwest China), PWE is closer to the rural exposure levels, and vice versa. The rural–urban differences were shrinking over the three decades, 1990–2019, but this is due to the faster urban O_3 growth instead of the rural air pollution decline.

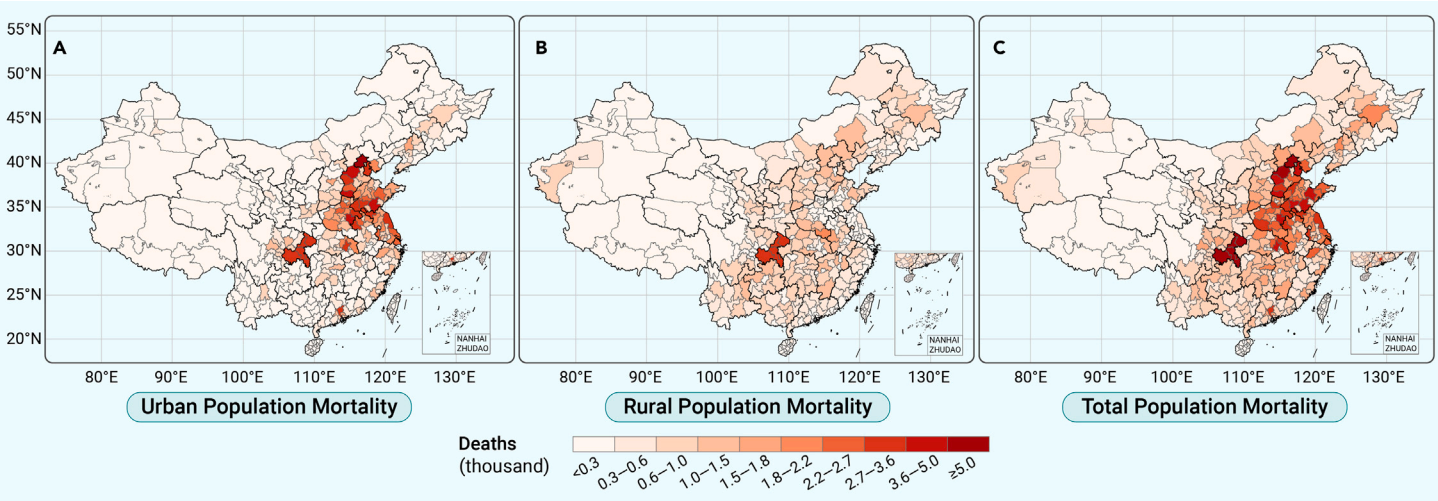

Figure 2. Mapping of ozone exposure-associated cardiopulmonary deaths in 2019 Excess cardiopulmonary mortalities are defined as the total deaths caused by chronic obstructive pulmonary disease and all-type cardiovascular diseases (COPD + CVDs). Numbers of premature deaths differentiate (A) urban, (B) rural, and (C) total population, and are aggregated to prefecture-level cities for mapping. Exposure-response curved relationships for COPD and cardiovascular mortality (see Figure S9) are estimated by exposure re-sampled meta-regression (see Method S5) considering 29 cohort-based epidemiological studies (see Table S9) identified from up-to-date systematic review. Color scale intervals are divided by Jenks natural breaks due to non-Gaussian and multi-peak mortality distribution. Regional statistics with multiple mortality metrics (death number, mortality rate, years of life lost) for 2019 are listed in Table 1, and statistics for 1990 are summarized in Table S2.

Hierarchical mortality cause identification attributable to ozone exposure

Previous long-term O_3 exposure-associated mortality (i.e., excess mortality) estimation studies did not consider cardiovascular deaths,[25,26] since relevant epidemiological studies exploring the risk association between O_3 exposure and cardiovascular mortality were rather rare, and contradiction existed among the sparse evidence.[27-30] However, after updating the systematic literature review to include more recent research into meta-analysis, we find a growing number of studies tending to take a stand that long-term O_3 exposure is also associated with additional premature death risks of ischemic heart disease (IHD) (RR = 1.021; 95% confidence interval [CI], 1.008–1.033) and total CVDs (RR = 1.024; 95% CI, 1.015–1.033). Newly published relevant cohort studies also update the mortality risks of COPD, all CRDs, and all non-communicable diseases (NCDs) (see Method S4 and Figures S3–S8). Therefore, we extend estimations onto tier-stratified multi-cause (tier 1: NCDs, tier 2: CRDs and CVDs, tier 3: COPD and IHD) O_3-induced excess deaths using optimized exposure-response curved relationships (see Method S5 and Figure S9), with three hierarchical mortality proportions calculated (Figure S10).

In 1990, COPD-induced mortality associated with long-term ambient O_3 exposure occupied 97.7% (95% UI: 95.6%–99.8%) of all-type CRD excess deaths, and the proportions remained constant over the 30 studied years (97.4%, 95% UI: 95.2%–99.5% in 2019). This verifies the coherency of the exposure-response risk associations for COPD and CRD mortalities, and indicates that COPD is the main cause of respiratory mortality—this is also why the Global Burden of Disease (GBD) 2019 study attributes all O_3 exposure-associated premature deaths to COPD.[23] Contrarily, IHD excess deaths accounted for 56.6% (53.8%–59.5%) of all-type cardiovascular deaths attributable to O_3 exposure in 1990, ascending monotonously to 90.9% (87.3%–94.7%) in 2019. This suggests that more cardiovascular mortality causes other than IHD can also be associated with long-term O_3 exposure (e.g., congestive heart failure[31]), and that IHD mortality rates soared disproportionally with these non-IHD CVDs, especially since 2000, resulting in such longitudinal cross-tier heterogeneity. Considering the high uncertainty in relative risks of IHD mortality drawn from limited cohort-based studies and other cardiovascular mortality causes potentially associated with O_3 exposure, we hence choose CVD excess mortality estimation as our main analysis.

Total CRD and CVD excess deaths made up 70.9% (95% UI: 68.7%–73.1%) of the proportion of NCD mortality attributable to long-term O_3 exposure in 2019, and it is noteworthy that the fraction in 1990 even erroneously exceeded 100%, indicating that the meta-estimated exposure-response relationships based on currently available evidence might not be sufficiently consistent across causes. The declining trend of the proportion reveals that mortality by other NCDs not associated with O_3 exposure (e.g., cancer) still increased, and thus estimations for long-term ambient O_3 exposure-associated NCD deaths might bring in unnecessary overestimation and unidentified uncertainties. Therefore, we decided to report the total excess cardiopulmonary mortality (specifically for CVDs and COPD) as our main results for the sake of full-scale mortality cause inclusion together with uncertainty restriction.

Excess cardiopulmonary mortality associated with ozone exposure

We map the excess cardiopulmonary deaths due to long-term O_3 exposure in 2019 aggregated by prefecture-level cities in Figure 2 (gridded mortality in Figure S11). The geographical distribution of the mortality approximately delineates Hu's Line (also known as the Heihe-Tengchong Line) dividing Southeast and Northwest China. Urban mortality clusters mainly in the metropolises and populous provinces with high ambient O_3 pollution (e.g., Shandong, Henan, Jiangsu), while rural mortalities are geographically distributed more evenly. In 2019, a total of 373.5 (95% UI: 240.6–510.9) thousand cardiopulmonary deaths were ascribed to long-term ambient O_3 exposure, among which urban excess mortality was 200.0 (128.9–273.6) thousand, and rural excess mortality was 173.5 (111.7–237.4) thousand (Table 1). The COPD excess mortality was 177.1 (120.4–239.5) thousand, and excess deaths induced from all-type CVDs were 196.4 (120.2–271.4) thousand. Mortalities in East China occupy around a third of the total deaths across the whole nation.

The O_3-attributable excess cardiopulmonary deaths accounted for 3.5% (2.3%–4.8%) of the overall Chinese mortality in 2019. In 1990, the total excess cardiopulmonary mortality was 292.0 (188.5–402.1) thousand, consisting of 3.5% (2.2%–4.8%) of the total mortality. Rural mortality was 209.900 (135.6–288.7) thousand, exceeding the urban O_3-attributable deaths by 127.8 (82.7–175.3) thousand (Table S2). Categorized by region, residence location, and mortality cause, the temporal trends of the estimated cardiopulmonary excess deaths associated with long-term O_3 exposure are shown in Figure 3. Total excess deaths increased by 3.3 (2.1–4.5) thousand per year, among which urban mortality climbed by 4.7 (3.0–6.4) thousand per year, while rural mortality shrank by 1.4 (0.9–1.9) thousand per year (Table S3). COPD mortality shows a decreasing trend by 1.0 (0.7–1.4) thousand per year due to the steady decline of cross-sectional mortality rates (Table S4), while the CVD mortality surged by 4.3 (2.8–6.0) thousand per year. Highest growths are observed in East and Central China while, in contrast, rates of change in Northwest China are insignificant.

Besides the number of excess deaths, which are strongly dependent on the population density, we also report the mortality rates adjusting the population to highlight the risks attributable to ambient O_3 exposure (Table 1). The average cardiopulmonary mortality rate over the Chinese population was 26.7 (17.2–36.5) per 100,000 in 2019. Specifically, urban population mortality rate was 23.6 (15.2–32.3) per 100,000, while rural mortality rate was higher at 31.4 (20.3–43.0) per 100,000. In earlier years, urban-rural divergences were greater. In most regions of China, rural residents suffer greater excess cardiopulmonary

Table 1. Regional and nationwide cardiopulmonary mortality metrics associated with long-term ozone exposure in 2019

	Excess deaths (thousands)			Mortality rates (per 100,000)			YLLs (million years)		
Region	Urban	Rural	Total	Urban	Rural	Total	Urban	Rural	Total
Northeast China	9.5	17.3	26.9	19.6	27.8	24.2	0.38	0.49	0.87
	(6.1–13.1)	(11.1–23.8)	(17.3–36.9)	(12.6–26.9)	(17.9–38.2)	(15.6–33.2)	(0.24–0.53)	(0.32–0.68)	(0.55–1.22)
North China	34.6	25.5	60.1	30.7	39.2	33.8	0.60	0.70	1.30
	(22.4–47.1)	(16.5–34.7)	(38.9–81.8)	(19.8–41.8)	(25.3–53.3)	(21.8–46.0)	(0.39–0.83)	(0.44–0.96)	(0.82–1.77)
East China	83.0	38.9	121.9	26.0	35.1	28.3	0.51	0.62	1.13
	(53.6–113.4)	(25.1–53.1)	(78.7–166.6)	(16.8–35.5)	(22.6–47.9)	(18.3–38.7)	(0.32–0.70)	(0.39–0.86)	(0.72–1.56)
Central China	41.0	30.3	71.2	27.6	34.4	30.1	0.54	0.61	1.15
	(26.4–55.9)	(19.5–41.3)	(45.9–97.2)	(17.8–37.7)	(22.2–46.9)	(19.4–41.1)	(0.34–0.75)	(0.39–0.84)	(0.72–1.58)
South China	14.2	15.2	29.4	14.6	24.9	18.6	0.29	0.45	0.74
	(9.1–19.7)	(9.7–20.9)	(18.8–40.6)	(9.3–20.2)	(16.0–34.3)	(11.9–25.6)	(0.18–0.40)	(0.27–0.61)	(0.46–1.02)
Northwest China	4.7	17.0	21.6	15.2	28.4	23.9	0.30	0.51	0.81
	(3.0–6.4)	(10.9–23.3)	(13.9–29.7)	(9.7–20.9)	(18.3–39.0)	(15.4–32.9)	(0.19–0.41)	(0.32–0.70)	(0.51–1.11)
Southwest China	13.0	29.3	42.3	14.6	28.0	21.8	0.29	0.49	0.78
	(8.3–17.9)	(18.8–40.2)	(27.1–58.2)	(9.3–20.1)	(18.0–38.5)	(14.0–30.0)	(0.18–0.40)	(0.31–0.69)	(0.49–1.09)
Nationwide	200.0	173.5	373.5	23.6	31.4	26.7	2.91	3.87	6.78
	(128.9–273.6)	(111.7–237.4)	(240.6–510.9)	(15.2–32.3)	(20.3–43.0)	(17.2–36.5)	(1.84–4.01)	(2.44–5.34)	(4.28–9.35)

Three mortality metrics are estimated as (1) the number of excess deaths in thousands, (2) age-standardized mortality rate per 100,000, and (3) years of life lost (YLLs) in million years. We only regard premature deaths as health outcomes from long-term ozone exposure in our study, so that disability-adjusted life years (DALYs) are equal to YLLs, for years of healthy life lost due to disability (YLDs) are considered constantly to be 0 (DALYs = YLLs + YLDs). Estimates are summarized by median with 95% uncertainty intervals (UIs) from 1,000-times Monte Carlo bootstrap simulation. Estimations of 1990 mortality metrics are summarized in Table S2.

mortality risks. Years of life lost (YLLs) (equal to the disability-adjusted life years when focusing merely on mortality) attributed to O_3 exposure was 6.78 (4.28–9.35) million in 2019, and specifically 2.91 (1.84–4.01) million years for urban population and 3.87 (2.44–5.34) million years for rural population. YLLs show a descending trend by 0.06 (0.04–0.09) million years per decade, even given the increase of excess mortality, as the life expectancy of Chinese population has significantly prolonged in the past three decades owing to the substantial improvement of the medical care system.[32]

Regulations are being made and revised to protect public health. The National Ambient Air Quality Standards (GB3095-2012) enacted by The Ministry of Environmental Protection of China (MEPC) since 2012 stipulate the Level-I standard as 100 $\mu g/m^3$ (equivalent to ~51.0 ppb), which is in accordance with the previous version of WHO Air Quality Guidelines (AQG2005),[33] and Level-II transitional standard as 160 $\mu g/m^3$ (equivalent to ~81.6 ppb). Taking 2019 as an example, if all regions suffering O_3 higher than Level-II were set to be exposed to 81.6 ppb, then only 14.2% of the excess premature deaths could have been avoided; while realizing Level-I standard could have effectively reduced 75.3% of the excess mortality, among which rural mortality could have been prevented by 84.1%, emphasizing the importance of achieving the planned O_3 control target. The stricter provision on warm-season peak O_3 pollution level, 60 $\mu g/m^3$ (equivalent to ~30.6 ppb) is added in AQG2021 for the first time,[33] based on the new evidence of long-term effects on all-cause and respiratory mortality. Realization of this ultimate goal can theoretically prevent all excess mortalities induced by long-term O_3 exposure, as the standard is below the threshold level (40–50 ppb, see Figure S9) synthesized from currently available epidemiological evidence.

Insights on driving factors of mortality change

Figure 4 sorts the provinces (including the municipalities) by O_3 exposure-associated excess cardiopulmonary deaths. For urban mortality (Figure 4A), the top 5 provinces, Shandong, Henan, Jiangsu, Hebei, and Anhui, have prevailed over the 30 years due to the dense urban population. Comparatively, ranking of rural mortality attributable to ambient O_3 exposure shows more of a shuffled pattern (Figure 4B). Multiple factors can influence the O_3-associated mortality change, as illustrated in Figure 5, decomposing the excess mortality change between 1990 and 2019 down to O_3 exposure change, population growth, population aging, overall cross-sectional mortality rate change, and urbanization-oriented population migration. The increments in ambient O_3 exposure (32.4%), total population (24.6%), and the vulnerable population proportion defined as the fraction of age ≥25 (13.4%) add on to the mortality increase, which are compromised by the declines in overall cross-sectional mortality rates (−11.2%), and population migration from rural to urban residence (−34.5%), leading to the overall mortality increasing rate by 24.7% for the entire population.

It is noteworthy that contributions from urbanization-oriented population migration act as a significant role in mortality change, which is overlooked in previous studies. Given that ambient O_3 pollution is generally lower in urban environments, population-weighted O_3 exposure can be reduced when a large proportion of rural residents migrate to cities, resulting in a reduction of total mortality. The effect of population migration takes the predominant role in moderately developed regions, such as Northwest provinces, while deterioration of ambient O_3 pollution and population growth carried the decisive weight in highly developed areas, such as Beijing, Shanghai, and Guangdong (Figure 5).

The antagonism between the growing ambient O_3 and population migration reveals the blind spot of using the PWE metric to quantify the population exposure that some regions specifically show low increasing or even decreasing tendency of PWE (Figure S12) should not be ascribed to the alleviation of ambient O_3 pollution, but the population migration to cities, even if both the urban and rural O_3 pollutions are elevating (e.g., Sanya in Hainan Province, urban O_3 rose from 46.7 to 50.3 ppb and rural O_3 climbed from 61.1 to 63.2 ppb, but the rural population proportion nose-dived from 70.3% to 17.7%, causing −5.9 ppb change in PWE). Such a phenomenon is mainly observed in vast territory cities in remote areas with lower annual pollution increasing rates but significant urbanization progress. In a nutshell, we aim to highlight the urban-rural O_3 exposure injustice for environmental policymakers—rural populations are persistently suffering from higher and ever-increasing O_3 exposure, despite the fact that rural-to-urban migration has been decreasing the ascending rate of overall exposure-associated excess mortality risks.

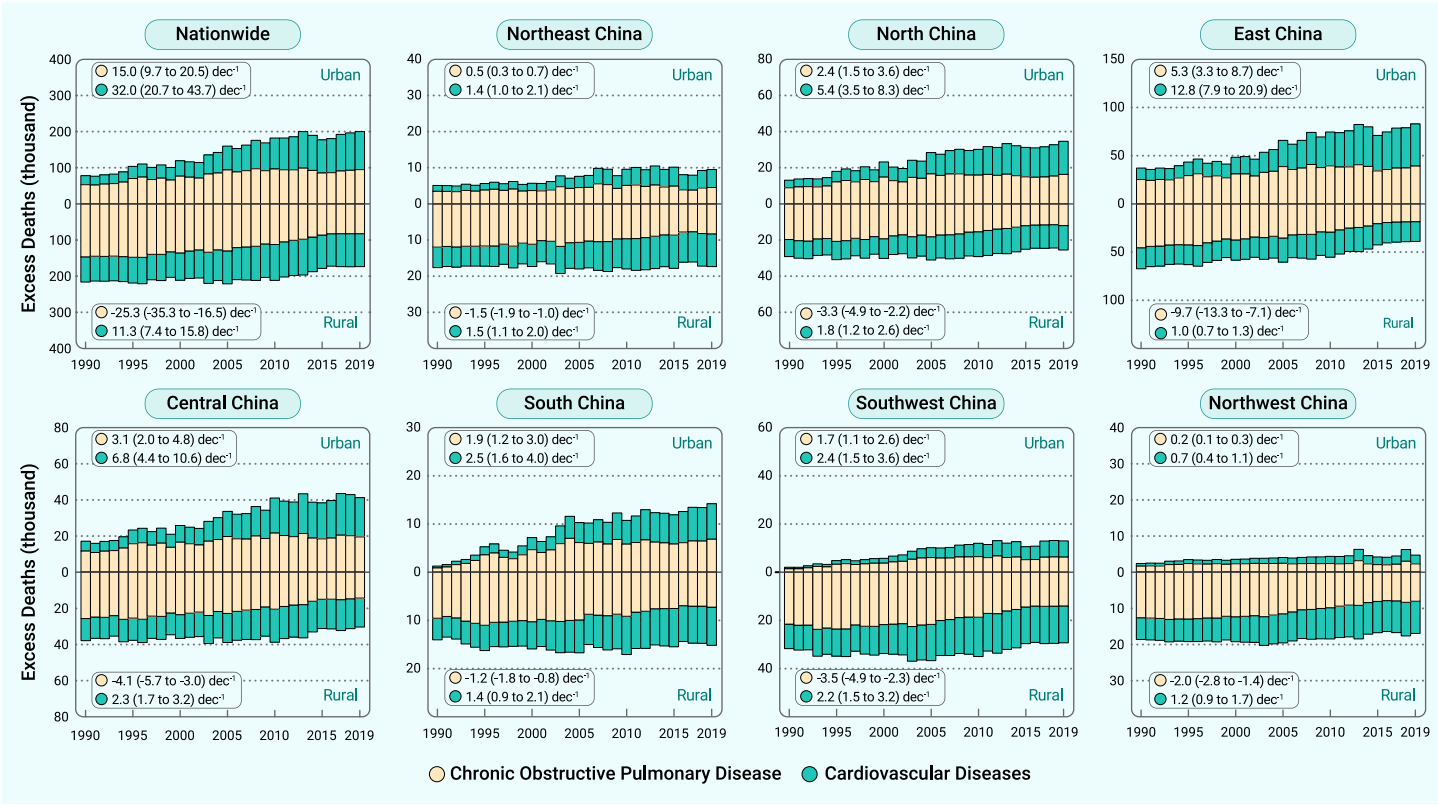

Figure 3. Thirty-year trends of national and regional urban-rural disaggregated excess cardiopulmonary deaths associated with long-term ozone exposure Total premature death numbers, aggregated for nationwide and seven geographical regions, are presented by piling up of mortality causes: COPD and all-type cardiovascular diseases. The upper part above the baseline in each subplot indicates urban population mortalities, and the lower part represents premature deaths on rural residents. Thirty-year longitudinal change rates with 95% confidence intervals (CIs) (1,000 deaths per decade) for 4 mortality indices (i.e., urban COPD, urban CVD, rural COPD, and rural CVD) as inserted are estimated by log-linear meta-regression models considering the central mortality estimates together with uncertainties derived from Monte Carlo bootstrap simulation. See Table S3 for detailed statistics of temporal trends of multiple mortality metrics.

DISCUSSION

To the best of our knowledge, this is the first study systematically assessing the long-term O_3 exposure-associated multi-cause (especially cardiopulmonary) excess mortality in China over the 30 historical years (1990–2019). We use a high-spatial-resolution ambient O_3 concentration dataset to quantify population O_3 exposure, and machine learning-based data fusion supervised by *in situ* observation can effectively reduce the O_3 estimation biases.[16-19] The urban-rural differentiation can more precisely characterize the environmental inequality that rural residents contribute less anthropogenic emissions of O_3 precursors, but suffer from higher O_3 exposure. We collect, review, and pool the most up-to-date epidemiological evidence on cause-specific mortality risks, including cohort studies on Chinese population to constrain bias from ethnical heterogeneity.[34,35] Synthesized from all qualified evidence, we conclude that long-term O_3 exposure is associated with both respiratory and cardiovascular mortality, while conventional mortality estimation studies, such as the GBD 2019 report,[23] overlooked the chronic respiratory risk, which might have severely underestimated the factual premature deaths (e.g., cardiovascular premature deaths occupied over half of total cardiopulmonary mortality in 2019). We highlight these blind points to arouse public attention that ambient O_3 hazards might have been underrated, and rural residents should be more aware of their O_3 exposure.

There are four major causes leading to higher rural O_3 pollution beyond the urban NO_X transporting to rural communities. First, it is important to note that NO_X emissions are more pronounced in urban environments, leading to increased O_3 scavenging by NO from traffic emissions, a phenomenon often referred to as the "NO_X titration trap." Second, urban areas tend to have higher aerosol concentrations, which can hinder solar radiation and thus limit photolytic reactions; additionally, these aerosols can serve as a sink for HO_x radicals and HNO_3, effectively suppressing O_3 formation.[36,37] Third, rural regions typically experience elevated biogenic VOC emissions due to the greater expanse of vegetation.[4] Finally, rural areas exhibit higher CO emissions, primarily due to the incomplete combustion of solid fuels, which are commonly used in China. This increased CO emission contributes to the generation of radicals that facilitate the oxidation of NO, thereby further augmenting O_3 formation.[38] Spatial patterns of the localized rural-urban O_3 differences (i.e., contrasting the rural ambient O_3 concentration with the adjacent urban O_3 level) are associated with a collection of sociodemographic and ecological features (Table S5), coinciding with the proved mechanisms.

Pre-existing studies only considered excess respiratory mortality associated with O_3 exposure because earlier evidences on cardiovascular mortality risk were contradictive. For instance, studies on ACS CPS II cohort estimated a protective effect on ischemic heart disease,[28] which neutralized the risks reported by other studies.[29] As a precursor of O_3, NO_2 concentrations are found to be anti-correlated with O_3, and such collinearity can erroneously misconceive the O_3-mortality relationship in multivariate regression analysis. We thus do not include studies in which mortality risks due to O_3 exposure are concealed by adjusting NO_2 exposure into meta-analysis.[39] In the Integrated Science Assessment for Ozone and Related Photochemical Oxidants (referred to as ISA2020, EPA/600/R-20/012) released by the US EPA in 2020, it is concluded that "the body of evidence is suggestive of, but not sufficient to infer, a causal relationship between long-term O_3 exposure and total mortality" based on evidence published by March 2018.[40] However, after reviewing the latest epidemiological evidence, we have decided to act as whistleblowers to push the envelope and emphasize the potential additional risk of long-term O_3 exposure on cardiovascular mortality. As outlined in the Clean Air Act, ISAs are scheduled to be updated every 5 years due to the evolving nature of science (https://www.epa.gov/air-research/research-health-effects-air-pollution). We have taken a step ahead of the US EPA in conducting evidence evaluations of the long-term O_3 exposure induced cardiovascular mortality risks at the epidemiological level.

The O_3 exposure-cardiovascular mortality association is pathologically plausible as verified in previous studies. Inhaled O_3 can trigger systemic inflammatory responses in the circulatory system,[41] provoke coagulation, platelet dysfunction, and endothelial injury,[42] elevate oxidative stress of the cardiovascular system,[43] and induce progressive thickening of the carotid arteries to restrict blood circulation.[44] In addition, short-term epidemiological studies focusing on acute O_3 exposure revealed strong association with a variety of cardiopulmonary symptoms,[5]

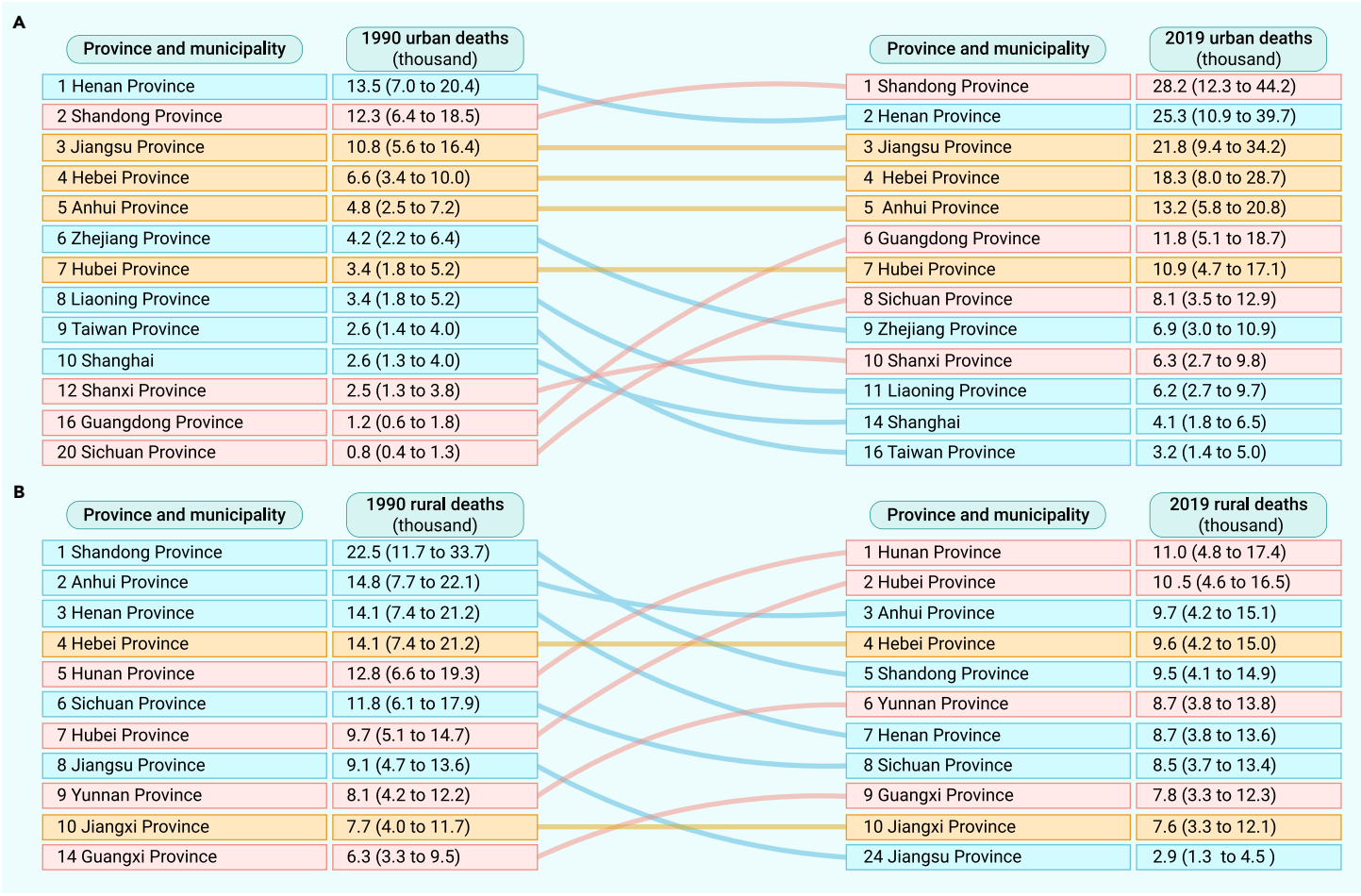

Figure 4. Leading 10 provinces and ranking changes of excess cardiopulmonary deaths from 1990 to 2019 Provinces altogether with municipalities are ranked in descending order separately for urban (A) and rural (B) populations according to the numbers of excess cardiopulmonary deaths (scaled in thousands with 95% UIs estimated by Monte Carlo bootstrap simulation) attributable to long-term ambient ozone exposure.

and thus it is sufficiently reasonable to assume that O_3 exposure increases the cardiovascular mortality risk.

We show that ambient O_3 pollution in China manifests a steadily climbing tendency, even given that the landmark National Air Quality Action Plan came into force in 2013.[45] This can be ascribed to the nonlinear relationships between the O_3 budget and emissions of precursors and the side effect of controlling particulate matter. Previous studies have verified that high-O_3 pollution cities follow the VOC-limited regime, indicating that reducing VOC will be more effective in abating O_3 pollution than controlling NO_X emission.[46] In addition, the effective control of aerosols could have increased solar radiation, and consequently accelerated tropospheric photolysis to boost O_3 formation.[47] But, fortunately, O_3-NO_X-VOC relationships have been approaching the transitional regime in metropolises such as Beijing as the relevant policies have been consistently implemented,[48,49] and hence we anticipate ambient O_3 pollution will decline in the near future.

We highlight the urban-rural environmental injustice in terms of ambient O_3 exposure, and also stress the antagonism between the climbing pollution levels and urbanization-oriented population migration on total population mortality. Our findings emphasize that, although high-speed urbanization has been pursued, government policymakers should never be blinded by the moderated growing rate of total population excess deaths attributable to long-term O_3 exposure, as rural residents suffer from ever-growing mortality risks due to higher air pollution exposure. Besides, exposure to particulate matter is also of urban-rural inequality among the Chinese population, as solid fuels have been widely used among rural residents during the past several decades, which can generate additional household exposure.[50] China has launched a rural clean heating campaign to reduce particulate matter pollution,[51] but there are still no policies specifically focusing on rural O_3 control. Therefore, special attention is urgently needed for rural residents to promote their environmental health equality. We strongly recommend that cities in which a substantial population of rural inhabitants reside in the downwind areas of urbanized districts, adopt strict measures to control diurnal anthropogenic NO_x emissions to curtail the urban-to-rural transfer of precursors. In addition, meteorological factors should be considered to enhance the efficacy of O_3 pollution control measures.

We encourage future research on four important areas. First, overall cause-specific mortality rates are highly affected by regional socioeconomic status, resulting in un-neglectable urban-rural divergence and geographical variability. In this study, we make a compromise to use country-level metrics provided in the GBD 2019 report due to the unavailability of province-level statistics throughout the 30 studied years. However, China CDC is endeavoring to release localized statistics, and relevant studies can be enhanced in the near future. Second, residential attribution is actually not simply as binary, as there are more sophisticated categorizations (e.g., urban, suburban, peri-urban, and rural). We analyzed the localized urban-rural O_3 discrepancy benefiting from urban-rural classified *in situ* observations and population distribution, and we need more precise classification to update the habitation-differentiated estimations and evaluate the effect on regional environmental health. Third, it will be valuable to keep tracking the ambient air pollution. We hanker after high-quality ambient air pollution databases from satellite-based remote-sensing measurements and CTM simulations, and more competitive data fusion algorithms to capture the population exposure with higher credibility are always appreciated. Finally, we need more nationwide cohort studies for multi-cause mortality risk estimation, so as to strengthen the representativeness of the pooled risk associations on Chinese population. The association between cardiovascular mortality risk and long-term ambient O_3 exposure is still in need of justification by follow-up studies. Prospective cohort studies in China are thriving in recent years, which can fill the literature gap and promote multi-region health studies.

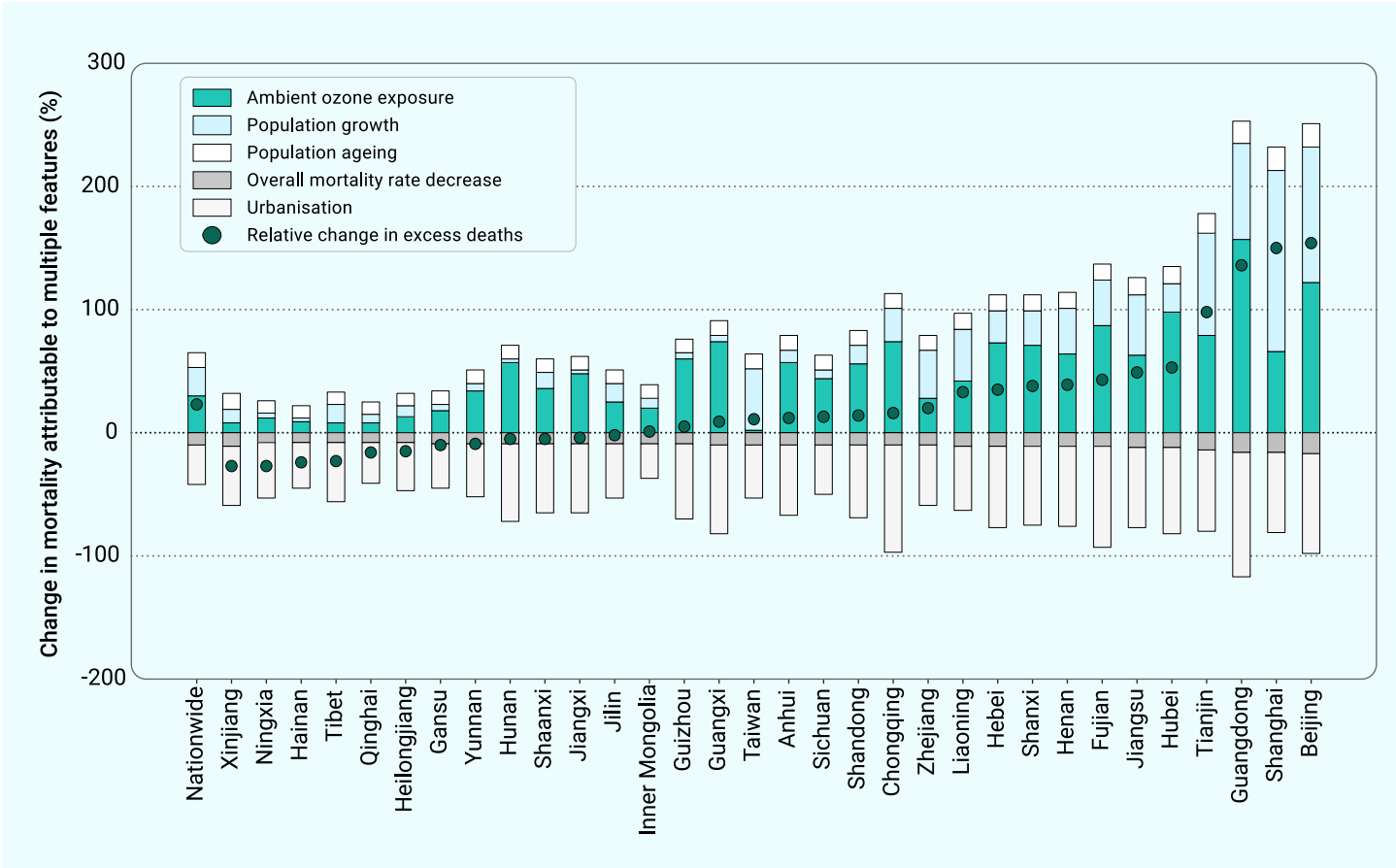

Figure 5. Contribution decomposition of nationwide and province-level relative changes in long-term ozone exposure-associated excess deaths from 1990 to 2019 Five contribution components are considered to be responsible for relative mortality changes as changes in (1) warm-season ambient ozone exposure levels, (2) total population, (3) population structure (e.g., aging), (4) cross-sectional overall mortality rates of COPD and cardiovascular diseases, and (5) urbanization. Urbanization is approximated by population fractions of urban residents. Independent contributions from each factor are dissociated by step-by-step feature substitution method, as shown by the stacked bars for the nationwide average and each province or municipality. Circles mark the overall relative change percentages of total cardiopulmonary mortalities from 1990 to 2019, which are equal to the sum of five influencing factors. Hong Kong and Macao are not analyzed as these two special administrative regions have fully accomplished urbanization since 1990 and thence effects from population migration cannot be dissociated.

MATERIALS AND METHODS

Urban-rural differentiated ambient O_3 tracking

The core basis ambient O_3 concentration tracking database with urban-rural distinguishment was developed by a two-stage space-time Bayesian neural network framework, consisting of first-stage multi-model ensembler (BayNNE)[16] and second-stage downscaler (BayNND).[17] BayNNE integrated eight fully coupled free-running simulations from CMIP6-endorsed Earth system models with interactive chemistry and chemistry-climate feedbacks, assisted with over 40 auxiliary predictors including sociodemographic, ecological, and emission features,[17] improved from the previously published version (see details in Method S1). The target spatial resolution was set at 1° × 1°, capturing the cell-average ambient O_3 concentrations with intra-cell variabilities smoothed. Predictions of cell-average concentrations ($\overline{C}$) followed Equation 1, which were the basis for further downscaling. In the equation, $M^{(i)}$ refer to simulations by different models, and subscripts *loc* and *t* represent spatial locations (by coordinates) and temporal nodes (by month), respectively.

$$\overline{C}_{loc,t} = \sum \alpha^{(i)}_{loc,t} \cdot M^{(i)}_{loc,t} + \beta_{loc,t} + \sigma_{loc,t} \quad \text{(Equation 1)}$$

BayNND predicted ambient O_3 concentrations from BayNNE-generated cell-level averages concentrations in 1/8° × 1/8° spatial resolution with stacked urban-rural differentiation. The "stacked" downscaling algorithm encapsulated urban- and rural-averaged ambient O_3 concentrations into each spatial cell, assigning all urban (or rural) population in each cell uniformly with a cell-specific urban (or rural) prediction (see Figure S13 for visual illustration). The schematic diagram of two-stage Bayesian neural network algorithms was conceptualized in Figure S14, and mathematical forms of BayNND are demonstrated in Equations 2 and 3, where *BayNN* represents Bayesian neural network regressor, *e* for Bayesian estimation ensemble member, *res* for urban/rural classification, s_i for three spatial indicators, t_i for three temporal indicators, and *a* for auxiliary predictors. The parameter family $\boldsymbol{\theta}$ including α_i, β, σ, k, and δ were predicted from ensemble averages by Markov-chain Monte Carlo method for Bayesian neural network.

$$C^{(res)}_{loc,t} = k^{(res)}_{loc,t} \overline{C}_{loc,t} + \delta^{(res)}_{loc,t} \quad \text{(Equation 2)}$$

$$\boldsymbol{\theta}^{(res)}_{loc,t,e} = \overline{BayNN^{(res)}_{e}(s_1, s_2, s_3, t_1, t_2, t_3, a_1, a_2, \cdots)} \quad \text{(Equation 3)}$$

Data fusion

Besides the BayNND, we fused three additional peer-reviewed high-quality data products[18-20] to realize an enhanced 30-year historical monthly averaged ambient O_3 concentration database spanning 1990–2019. The first 0.1° × 0.1° elemental dataset was developed by M^{3}Fusion (multi-scale, multi-modal, and multi-temporal fusion) machine learning algorithm and the conventional Bayesian maximum entropy statistical method in sequence (M^3-BME) to assimilate nine observation-nudged CTM simulations.[20] Covering 30 years, the calibration-observation accuracy is high to R^2 = 0.81, RMSE = 4.0 ppb after space-time correction.

One ambient O_3 product was constructed using a cluster-enhanced ensemble machine learning (CEML), training region-exclusive algorithms to retain the geographical variability.[18] CEML mixed the results from chemistry reanalysis and remote sensing, with over 80 supplemental geographical and meteorological features, to realize 0.5° × 0.5° monthly resolved ambient O_3 concentrations across 2003–2019, with overall accuracy R^2 = 0.92, RMSE = 4.1 ppb.

The last base dataset supported by the team of Tracking Air Pollution in China (TAP), was produced by random forest regressor with stochastic spatial auto-correlation signal compensation.[19] TAP utilized CTM simulations and satellite remote-sensing measurements to realize near real-time 0.1° × 0.1° daily prediction since 2013, achieving accuracy as

R^2 = 0.70, RMSE = 13.3 ppb. All three data products measured the ambient O_3 in metric of daily maximum 8-h average. Detailed procedures were precisely delineated in the original literature.[18-20]

Fusing multiple databases supervised by *in situ* observations can restrict biases from any single approach. As all four ambient O_3 tracking products had achieved high consistency with the observations, we used an elastic net regressor to fuse BayNND, M^3-BME, CEML, and TAP, assisted with three spatial and three temporal indicators,[17] to avoid overfitting. Detailed phased procedures for data fusion were illustrated in Method S2. Finally, by highlighting the peak exposure (April to September), 6-month ozone-season daily maximum 8-h average (OSDMA8) was calculated for mortality estimation. The Bayesian neural networks were constructed on Python-package TensorFlow (version 2.3.1), and elastic net regressions were performed by scikit-learn (version 0.23.2).

Ground-level observations for supervised training and validation

We used stationary observations as labels for all-stage supervised model training and accuracy evaluation. The urban-rural distinguished *in situ* observations were obtained from the TOAR archives[10] and CNEMC.[11] TOAR recognized 3,610 urban and 3,206 rural sites based on population density by remote sensing; CNEMC identified 1,777 urban and 245 suburban sites by administrative district division, whereas 245 suburban-labeled sites were reclassified as rural sites throughout this study, as (1) the observed "suburban"-labeled ambient O_3 concentrations were closer to the predicted rural concentrations (R^2 = 0.81, normalized mean bias, NMB = 2.8%) than urban predictions (R^2 = 0.48, NMB = −11.6%, details in Figure S15), and (2) the projected population density of 2019 of the suburban-labeled sites were way lower than 1,500 people per km^2, the urbanization standard (Content S1).

In the first-stage multi-model fusion, 1° × 1° gridded cell-average concentrations including all available sites excluding CNEMC stations (cell-average levels could be urban-biased due to disproportional deployment in urban and rural environments) were used as supervision labels for model training. The global-scale overall fitting accuracy was R^2 = 0.94, RMSE = 2.6 ppb by metric of monthly averaged daily 8-h maximum, and the evaluation of 10-fold cross-validation test showed R^2 = 0.90.

In the second-stage 1/8° × 1/8° gridded downscaling with urban-rural differentiation and third-stage data fusion, we used urban- and rural-labeled observations for model training. Throughout the studied 30 years globally, accuracy of urban predictions was R^2 = 0.90, RMSE = 3.8 ppb (cross-validation R^2 = 0.85), and R^2 = 0.92, RMSE = 5.6 ppb (cross-validation R^2 = 0.88) for rural predictions in the second-stage BayNND.

For the latest 6 years (2014–2019), prediction accuracies were evaluated with observations in China, as R^2 = 0.91, RMSE = 4.2 ppb (cross-validation R^2 = 0.82) for urban, and R^2 = 0.89, RMSE = 5.2 ppb (cross-validation R^2 = 0.86) for rural predictions by the third-stage data fusion algorithm. The 10-fold methodological cross-validation tests on Chinese sites during 2014–2019 revealed $R^2 \geq 0.82$, RMSE ≤ 7.0 ppb, and 30-year global overall accuracy of the final dataset was R^2 = 0.92, RMSE = 4.4 ppb (Table S6). Spatiotemporal generalizability kept satisfactory across all designed tests (Method S8 and Table S7).

Risk association quantification

We updated the latest published systematic review[9] up to October 2022 to collect all recently published cohort-based epidemiological evidence on risk association between long-term O_3 exposure and multi-cause mortalities. We searched four additional qualified studies,[34,35,52,53] and by Quality Assessment Tool of Observational Cohort and Cross-Sectional Studies developed by NIH (Table S8), all these newly added studies were categorized as "Good" (Table S9).

We applied the Hunter-Schmidt meta-analysis estimator to pool the relative risk values reported by multiple studies, based on which mortality causes with significant positive pooled risks were then considered for further mortality estimation in this study. We finally identified NCDs (RR = 1.016; 95% CI, 1.011–1.021), CRDs (RR = 1.020; 95% CI, 1.006–1.035), together with COPD (RR = 1.056; 95% CI, 1.029–1.084) as a subordinate respiratory disease, and CVDs (RR = 1.024; 95% CI, 1.015–1.033) with its subset, IHD (RR = 1.021; 95% CI, 1.008–1.033), as mortality causes associated with long-term O_3 exposure, by meta-analysis (see Method S4 and Figures S3–S7 for details). The meta-analysis results were assessed to be of "High" credibility by the Grading of Recommendations Assessment, Development, and Evaluation system (Tables S10–S14).[54]

To capture the potential nonlinear trends of exposure-mortality associations more precisely, the concentration-response curves for the five identified mortality causes were constructed by meta-regression enhanced with exposure range resampling (see Method S5).[9] Concentration-response curves provided by the original literature were preferred in priority, while for studies not reporting the curves, linear trends were presumed by setting the lowest 5th percentile exposure concentration as the theoretical minimum risk exposure level for resampling (see Table S15).[55] The cause-specific curve-based relative risk values as a function of exposure concentration (RR_x, see Figure S9) are adopted for O_3 exposure-attributable excess mortality estimation as main analysis.

Population gridding and calibration

We integrated the population products included by the Socioeconomic Data and Applications Center (SEDAC) and China Statistical Yearbook series (1999–2020) released by National Bureau of Statistics to generate the calibrated gridded Chinese population dataset during 1990–2019. We applied a cubic spline model to extrapolate the two fundamental datasets, Gridded Population of the World (GPW) (version 4.11) and Population Dynamics with urban-rural specification (version 1.01), to the 30 consecutive study years for each grid. Next, we linearly calibrated the province-level populations aligning with the China Statistical Yearbook. The demographic age statistics were downloaded from GBD Population Estimates 1950–2019[56] and The China Statistical Yearbook series 2004–2019, with which the age-stratified risked population (age ≥25) were estimated. Grid-level male and female populations were additionally split according to the province-level gender ratio reported in the China Statistical Yearbook for further sensitivity analysis.

The urban-rural binary classification for each cell resided with habitants was based on the population density of each 30″ × 30″ fine cell: >1,500 people per km^2 as urban and <1,500 people per km^2 as rural. When upscaling to 1/8° × 1/8° coarser cell, the urban and rural residents were summed up separately and stacked in each coarse cell. The reason for gridded population upscaling is the spatial resolution limitation of ambient O_3 tracking (approximately 10 × 10 km^2). A schematic illustration for urban-rural stacked upscaling is shown in Figure S16. The ultimate annually resolved population dataset with 1/8° × 1/8° spatial resolution encapsulated four counts of population in each grid: (1) rural male, (2) rural female, (3) urban male, and (4) urban female. Detailed procedures are explained in the Method S6 and Figure S17.

The definition of urbanization throughout the study is cell-level proportion of urban residents among all population. Due to data unavailability, we did not track the individual-level migration behavior, whereby rural-to-urban population migration was reflected in a cross-sectional level by change of the urban-rural population structure, as illustrated in Figure S18. A demonstrative diagram for stacked population exposure assignment (i.e., cell-based concentration-population projection) is given in Figure S19. The cell-level PWE from ambient O_3 concentration of x was calculated by Equation 4, suitable for urban, rural, and total populations.

$$PWE = \frac{\sum_{res} x_{res} \cdot Pop_{res}}{\sum_{res} Pop_{res}} \quad \text{(Equation 4)}$$

Excess mortality estimation

We estimated the O_3 exposure-attributable excess mortalities by linking ambient O_3, concentration-response association, population, and cross-sectional mortalities together. For the population at risk (i.e., age ≥25), the population attributable fraction (AF) at specific ambient O_3 concentration of x followed

$$AF = \frac{RR_x - 1}{RR_x} \quad \text{(Equation 5)}$$

with which the cell-level excess deaths, $\Delta Mort$, and attributable YLLs, $\Delta YLLs$, were estimated as

$$\Delta Mort = \sum_{res}\sum_{age} y_{0\,age} \cdot AF_{res} \cdot Pop_{age,res} \quad \text{(Equation 6)}$$

$$\Delta YLLs = \sum_{res}\sum_{age} YLLs_{0\,age} \cdot AF_{res} \cdot Pop_{age,res} \quad \text{(Equation 7)}$$

where y_0 and $YLLs_0$ are the cause-specific cross-sectional mortality rate and rate of YLLs (per 100,000), respectively; and Pop is the cell-level population at risk. Subscript age refers to the age-stratified group by 5-year intervals from 25 to ≥95 (i.e., 25–29, 30–34, …, 90–94, and ≥95) corresponding to the estimates of mortality rate provided by Institute for Health Metrics and Evaluation (IHME), and due to data unavailability, age structure is assumed to be the same for urban and rural populations; AF_{res} is calculated from urban-rural distinguished ambient O_3 concentrations. The cross-sectional annual age- and gender-standardized mortality statistics of the five studied causes were collected from the GBD Results portal. The cell-level estimations were specified for urban and rural residents, given distinguished ambient O_3 exposure and population.

Mortalities were estimated by 1,000 realization Monte Carlo bootstrap, accomplished in Python (version 3.8.0). Considering the skewed distribution, medians are extracted to

represent the central levels other than the arithmetic means, together with 95% UIs. Global distributions of the results were mapped via QGIS (version 3.26). Sensitivity analyses were enclosed in Method S7.

Other involved analysis

Grid-level results were aggregated into seven administrative geographical divisions (Northeast, North, East, Central, South, Southwest, and Northwest China) and four world-class megalopolises (Jing-Jin-Ji, Cheng-Yu, Yangtze River Delta, and the Greater Bay Area) for statistics and interpretation. Further descriptions were expounded in Method S8 and Figure S1. Longitudinal trends of O_3 concentrations were calculated by generalized linear model, and trends of estimated mortality metrics with 95% UIs were calculated by log-linear meta-regression with a random-effects estimator, conducted in R package *metafor*. Association assessment of driving factors on rural-urban ambient O_3 disparity was realized by generalized multivariate linear regression model, and feature screening was conducted by forward stepwise selection setting significant threshold as $p < 0.2$. Literature-based external validations on the urban-rural differentiated ambient O_3 predictions were presented in Figure S20 and Content S2.

Source apportionments for the 1990–2019 mortality change rates were accomplished by controlling the relevant factors each-by-each, following the piling-up decomposition approach suggested by GBD 2015.[57] For each province, we calculated the percentage contributions of change rates in excess deaths from five independent factors: (1) effect of change in urban and rural ambient O_3 pollution level, (2) effect of population growth, (3) effect of population aging, leading to greater risked population, (4) effect of change in baseline mortality rate (i.e., cross-sectional mortality rate reported by IHME), and (5) effect of urbanization-oriented urban-rural population structure change (i.e., Chinese rural populations are migrating to urban living environments), among which the last factor is extended from previous studies. We added special treatment on the urban-rural exposure differentiation, as total excess mortality burdens in 1990 (year 1 as noted in the superscript) and 2019 (year 2) were calculated as demonstrated below.

$$\Delta Mort^{(1)} = \sum_{age}\sum_{res}\left(\sum_{age} Pop^{(1)}_{age,res} \times \frac{Pop^{(1)}_{age}}{\sum Pop^{(1)}_{age}} \times y0^{(1)}_{age} \times \frac{Pop^{(1)}_{res} \times AF^{(1)}_{res}}{\sum Pop^{(1)}_{res}}\right) \quad \text{(Equation 8)}$$

$$\Delta Mort^{(2)} = \sum_{age}\sum_{res}\left(\sum_{age} Pop^{(2)}_{age,res} \times \frac{Pop^{(2)}_{age}}{\sum Pop^{(2)}_{age}} \times y0^{(2)}_{age} \times \frac{Pop^{(2)}_{res} \times AF^{(2)}_{res}}{\sum Pop^{(2)}_{res}}\right) \quad \text{(Equation 9)}$$

We then defined the modified excess mortalities by substituting the influencing features step by step, as presented below.

$$A = \sum_{age}\sum_{res}\left(\sum_{age} Pop^{(2)}_{age,res} \times \frac{Pop^{(1)}_{age}}{\sum Pop^{(1)}_{age}} \times y0^{(1)}_{age} \times \frac{Pop^{(1)}_{res} \times AF^{(1)}_{res}}{\sum Pop^{(1)}_{res}}\right) \quad \text{(Equation 10)}$$

$$B = \sum_{age}\sum_{res}\left(\sum_{age} Pop^{(2)}_{age,res} \times \frac{Pop^{(2)}_{age}}{\sum Pop^{(2)}_{age}} \times y0^{(1)}_{age} \times \frac{Pop^{(1)}_{res} \times AF^{(1)}_{res}}{\sum Pop^{(1)}_{res}}\right) \quad \text{(Equation 11)}$$

$$C = \sum_{age}\sum_{res}\left(\sum_{age} Pop^{(2)}_{age,res} \times \frac{Pop^{(2)}_{age}}{\sum Pop^{(2)}_{age}} \times y0^{(2)}_{age} \times \frac{1 - AF^{(2)}_{res}}{1 - AF^{(1)}_{res}} \times \frac{Pop^{(1)}_{res} \times AF^{(1)}_{res}}{\sum Pop^{(1)}_{res}}\right) \quad \text{(Equation 12)}$$

$$D = \sum_{age}\sum_{res}\left(\sum_{age} Pop^{(2)}_{age,res} \times \frac{Pop^{(2)}_{age}}{\sum Pop^{(2)}_{age}} \times y0^{(2)}_{age} \times \frac{Pop^{(1)}_{res} \times AF^{(2)}_{res}}{\sum Pop^{(1)}_{res}}\right) \quad \text{(Equation 13)}$$

From $\Delta Mort^{(1)}$ to A, we only changed the total population but maintained the age demographic and urban-rural structure, so that the dissociated contribution of population growth was calculated by Equation 14. We then replaced the age structure to observe the effect of population aging (Equation 15). Next, the baseline mortality rate was updated, where we should introduce a correction factor (Equation 12, the fourth term in the bracket), that the 2019 baseline mortality rate contains the part of contribution from changed O_3 exposure, from which we calculated the effect of baseline mortality rate change (Equation 16). Finally, the exposure-determined *AFs* were aligned to 2019 level, and we thus calculated the contribution from exposure change (Equation 17) and the remained urbanization-oriented population migration (Equation 18).

$$\text{Population growth effect (\%)} = \left(A - \Delta Mort^{(1)}\right) \Big/ \Delta Mort^{(1)} \quad \text{(Equation 14)}$$

$$\text{Population ageing effect (\%)} = (B - A)/A \quad \text{(Equation 15)}$$

$$\text{Baseline mortality rate change effect (\%)} = (C - B)/B \quad \text{(Equation 16)}$$

$$\text{Exposure change effect (\%)} = (D - C)/C \quad \text{(Equation 17)}$$

$$\text{Population migration effect (\%)} = \left(\Delta Mort^{(2)} - D\right) \Big/ D \quad \text{(Equation 18)}$$

REFERENCES

1. Wang, T., Xue, L., Brimblecombe, P., et al. (2017). Ozone pollution in China: A review of concentrations, meteorological influences, chemical precursors, and effects. Sci. Total Environ. ***575***, 1582–1596.
2. Hallquist, M., Munthe, J., Hu, M., et al. (2016). Photochemical smog in China: scientific challenges and implications for air-quality policies. Natl. Sci. Rev. ***3***, 401–403.
3. An, Z., Huang, R.J., Zhang, R., et al. (2019). Severe haze in northern China: A synergy of anthropogenic emissions and atmospheric processes. Proc. Natl. Acad. Sci. USA ***116***, 8657–8666.
4. Laothawornkitkul, J., Taylor, J.E., Paul, N.D., et al. (2009). Biogenic volatile organic compounds in the Earth system. New Phytol. ***183***, 27–51.
5. Zheng, X.Y., Orellano, P., Lin, H.L., et al. (2021). Short-term exposure to ozone, nitrogen dioxide, and sulphur dioxide and emergency department visits and hospital admissions due to asthma: A systematic review and meta-analysis. Environ. Int. ***150***, 106435.
6. Ji, M., Cohan, D.S., and Bell, M.L. (2011). Meta-analysis of the Association between Short-Term Exposure to Ambient Ozone and Respiratory Hospital Admissions. Environ. Res. Lett. ***6***, 024006.
7. Liu, Y., Pan, J., Fan, C., et al. (2021). Short-Term Exposure to Ambient Air Pollution and Mortality From Myocardial Infarction. J. Am. Coll. Cardiol. ***77***, 271–281.
8. Zhao, R., Chen, S., Wang, W., et al. (2017). The impact of short-term exposure to air pollutants on the onset of out-of-hospital cardiac arrest: A systematic review and meta-analysis. Int. J. Cardiol. ***226***, 110–117.
9. Sun, H.Z., Yu, P., Lan, C., et al. (2022). Cohort-based long-term ozone exposure-associated mortality risks with adjusted metrics: A systematic review and meta-analysis. Innovation ***3***, 100246.
10. Schultz, M.G., Schroder, S., Lyapina, O., et al. (2017). Tropospheric Ozone Assessment Report: Database and metrics data of global surface ozone observations. Elem. Sci. Anth. ***5***, 1–26.
11. Lu, X., Hong, J., Zhang, L., et al. (2018). Severe Surface Ozone Pollution in China: A Global Perspective. Environ. Sci. Technol. Lett. ***5***, 487–494.
12. Inness, A., Ades, M., Agustí-Panareda, A., et al. (2019). The CAMS reanalysis of atmospheric composition. Atmos. Chem. Phys. ***19***, 3515–3556.
13. Gong, P. (2012). Remote sensing of environmental change over China: A review. Chin. Sci. Bull. ***57***, 2793–2801.
14. Shen, H., Sun, Z., Chen, Y., et al. (2021). Novel Method for Ozone Isopleth Construction and Diagnosis for the Ozone Control Strategy of Chinese Cities. Environ. Sci. Technol. ***55***, 15625–15636.
15. Eyring, V., Bony, S., Meehl, G.A., et al. (2016). Overview of the Coupled Model Intercomparison Project Phase 6 (CMIP6) experimental design and organisation. Geosci. Model Dev. (GMD) ***9***, 1937–1958.
16. Sun, Z., and Archibald, A.T. (2021). Multi-stage ensemble-learning-based model fusion for surface ozone simulations: A focus on CMIP6 models. Environ. Sci. Ecotechnol. ***8***, 100124.
17. Sun, H., Shin, Y.M., Xia, M., et al. (2022). Spatial Resolved Surface Ozone with Urban and Rural Differentiation during 1990-2019: A Space-Time Bayesian Neural Network Downscaler. Environ. Sci. Technol. ***56***, 7337–7349.
18. Liu, X., Zhu, Y.J., Xue, L., et al. (2022). Desai AR, Wang HK. Cluster-Enhanced Ensemble Learning for Mapping Global Monthly Surface Ozone From 2003 to 2019. Geophys. Res. Lett. ***49***, e2022GL097947.
19. Xue, T., Zheng, Y., Geng, G., et al. (2020). Estimating Spatiotemporal Variation in Ambient Ozone Exposure during 2013-2017 Using a Data-Fusion Model. Environ. Sci. Technol. ***54***, 14877–14888.
20. DeLang, M.N., Becker, J.S., Chang, K.L., et al. (2021). Mapping Yearly Fine Resolution Global Surface Ozone through the Bayesian Maximum Entropy Data Fusion of Observations and Model Output for 1990-2017. Environ. Sci. Technol. ***55***, 4389–4398.
21. Xu, J., Ma, J.Z., Zhang, X.L., et al. (2011). Measurements of ozone and its precursors in Beijing during summertime: impact of urban plumes on ozone pollution in downwind rural areas. Atmos. Chem. Phys. ***11***, 12241–12252.
22. Tong, L., Zhang, H., Yu, J., et al. (2017). Characteristics of surface ozone and nitrogen oxides at urban, suburban and rural sites in Ningbo, China. Atmos. Res. ***187***, 57–68.
23. GBD 2019 Risk Factors Collaborators, Aravkin, A.Y., Zheng, P., et al. (2020). Global burden of 87 risk factors in 204 countries and territories, 1990-2019: a systematic analysis for the Global Burden of Disease Study 2019. Lancet ***396***, 1223–1249.
24. Lloyd, C.T., Sorichetta, A., and Tatem, A.J. (2017). High resolution global gridded data for use in population studies. Sci. Data ***4***, 170001.
25. Yin, P., Brauer, M., Cohen, A.J., et al. (2020). The effect of air pollution on deaths, disease burden, and life expectancy across China and its provinces, 1990-2017: an analysis for the Global Burden of Disease Study 2017. Lancet Planet. Health ***4***, e386–e398.
26. Malley, C.S., Henze, D.K., Kuylenstierna, J.C.I., et al. (2017). Updated Global Estimates of Respiratory Mortality in Adults ≥30 Years of Age Attributable to Long-Term Ozone Exposure. Environ. Health Persp. ***125***, 087021.
27. Jerrett, M., Burnett, R.T., Pope, C.A., III, et al. (2009). Long-term ozone exposure and mortality. N. Engl. J. Med. ***360***, 1085–1095.
28. Turner, M.C., Jerrett, M., Pope, C.A., III, et al. (2016). Long-Term Ozone Exposure and Mortality in a Large Prospective Study. Am. J. Respir. Crit. Care Med. ***193***, 1134–1142.

29. Crouse, D.L., Peters, P.A., Hystad, P., et al. (2015). Ambient $PM_{2.5}$, O_3, and NO_2 Exposures and Associations with Mortality over 16 Years of Follow-Up in the Canadian Census Health and Environment Cohort (CanCHEC). Environ. Health Persp. ***123***, 1180–1186.
30. Cakmak, S., Hebbern, C., Pinault, L., et al. (2018). Associations between long-term $PM_{2.5}$ and ozone exposure and mortality in the Canadian Census Health and Environment Cohort (CANCHEC), by spatial synoptic classification zone. Environ. Int. ***111***, 200–211.
31. Zanobetti, A., and Schwartz, J. (2011). Ozone and survival in four cohorts with potentially predisposing diseases. Am. J. Respir. Crit. Care Med. ***184***, 836–841.
32. Gong, P., Liang, S., Carlton, E.J., et al. (2012). Urbanisation and health in China. Lancet ***379***, 843–852.
33. World Health Organization (2021). WHO Global Air Quality Guidelines: Particulate Matter ($PM_{2.5}$ and PM_{10}), Ozone, Nitrogen Dioxide, Sulfur Dioxide and Carbon Monoxide (Geneva: World Health Organization).
34. Niu, Y., Zhou, Y., Chen, R., et al. (2022). Long-term exposure to ozone and cardiovascular mortality in China: a nationwide cohort study. Lancet Planet. Health ***6***, e496–e503.
35. Liu, S., Zhang, Y., Ma, R., et al. (2022). Long-term exposure to ozone and cardiovascular mortality in a large Chinese cohort. Environ. Int. ***165***, 107280.
36. Ivatt, P.D., Evans, M.J., and Lewis, A.C. (2022). Suppression of surface ozone by an aerosol-inhibited photochemical ozone regime. Nat. Geosci. ***15***, 536–540.
37. Li, K., Jacob, D.J., Liao, H., et al. (2019). Anthropogenic drivers of 2013-2017 trends in summer surface ozone in China. Proc. Natl. Acad. Sci. USA ***116***, 422–427.
38. Shen, G., and Xue, M. (2014). Comparison of Carbon Monoxide and Particulate Matter Emissions from Residential Burnings of Pelletized Biofuels and Traditional Solid Fuels. Energy Fuel. ***28***, 3933–3939.
39. Strak, M., Weinmayr, G., Rodopoulou, S., et al. (2021). Long term exposure to low level air pollution and mortality in eight European cohorts within the ELAPSE project: pooled analysis. BMJ ***374***, n1904.
40. U.S. EPA (2020). Integrated Science Assessment (ISA) for Ozone and Related Photochemical Oxidants (Final Report, Apr 2020) (Washington, DC: U.S. Environmental Protection Agency).
41. Day, D.B., Xiang, J., Mo, J., et al. (2017). Association of Ozone Exposure With Cardiorespiratory Pathophysiologic Mechanisms in Healthy Adults. JAMA Intern. Med. ***177***, 1344–1353.
42. Xia, Y., Niu, Y., Cai, J., et al. (2018). Effects of Personal Short-Term Exposure to Ambient Ozone on Blood Pressure and Vascular Endothelial Function: A Mechanistic Study Based on DNA Methylation and Metabolomics. Environ. Sci. Technol. ***52***, 12774–12782.
43. Kodavanti, U.P., Schladweiler, M.C., Ledbetter, A.D., et al. (2000). The spontaneously hypertensive rat as a model of human cardiovascular disease: evidence of exacerbated cardiopulmonary injury and oxidative stress from inhaled emission particulate matter. Toxicol. Appl. Pharmacol. ***164***, 250–263.
44. Wang, M., Sampson, P.D., Sheppard, L.E., et al. (2019). Long-Term Exposure to Ambient Ozone and Progression of Subclinical Arterial Disease: The Multi-Ethnic Study of Atherosclerosis and Air Pollution. Environ. Health Persp. ***127***, 57001.
45. Huang, J., Pan, X., Guo, X., et al. (2018). Health impact of China's Air Pollution Prevention and Control Action Plan: an analysis of national air quality monitoring and mortality data. Lancet Planet. Health ***2***, e313–e323.
46. Zhao, B., Wang, S.X., Liu, H., et al. (2013). NO_x emissions in China: historical trends and future perspectives. Atmos. Chem. Phys. ***13***, 9869–9897.
47. Ma, X., Huang, J., Zhao, T., et al. (2021). Rapid increase in summer surface ozone over the North China Plain during 2013–2019: a side effect of particulate matter reduction control? Atmos. Chem. Phys. ***21***, 1–16.
48. Liu, Z., Doherty, R.M., Wild, O., et al. (2021). Contrasting chemical environments in summertime for atmospheric ozone across major Chinese industrial regions: the effectiveness of emission control strategies. Atmos. Chem. Phys. ***21***, 10689–10706.
49. Wang, W., Parrish, D.D., Wang, S., et al. (2022). Long-term trend of ozone pollution in China during 2014-2020: distinct seasonal and spatial characteristics and ozone sensitivity. Atmos. Chem. Phys. ***22***, 8935–8949.
50. Shen, H., Tao, S., Chen, Y., et al. (2017). Urbanization-induced population migration has reduced ambient $PM_{2.5}$ concentrations in China. Sci. Adv. ***3***, e1700300.
51. Meng, W., Zhong, Q., Chen, Y., et al. (2019). Energy and air pollution benefits of household fuel policies in northern China. Proc. Natl. Acad. Sci. USA ***116***, 16773–16780.
52. So, R., Andersen, Z.J., Chen, J., et al. (2022). Long-term exposure to air pollution and mortality in a Danish nationwide administrative cohort study: Beyond mortality from cardiopulmonary disease and lung cancer. Environ. Int. ***164***, 107241.
53. Yuan, Y., Wang, K., Sun, H.Z., et al. (2023). Excess mortality associated with high ozone exposure: A national cohort study in China. Environ. Sci. Ecotechnol. ***15***, 100241.
54. Guyatt, G.H., Oxman, A.D., Vist, G.E., et al.; GRADE Working Group (2008). GRADE: an emerging consensus on rating quality of evidence and strength of recommendations. BMJ ***336***, 924–926.
55. Burnett, R.T., Pope, C.A., III, Ezzati, M., et al. (2014). An integrated risk function for estimating the global burden of disease attributable to ambient fine particulate matter exposure. Environ. Health Persp. ***122***, 397–403.
56. Global Burden of Disease Collaborative Network (2020). Global Burden of Disease Study 2019 (GBD 2019) Population Estimates 1950-2019 (Institute for Health Metrics and Evaluation (IHME)).
57. Cohen, A.J., Brauer, M., Burnett, R., et al. (2017). Estimates and 25-year trends of the global burden of disease attributable to ambient air pollution: an analysis of data from the Global Burden of Diseases Study 2015. Lancet ***389***, 1907–1918.

ACKNOWLEDGMENTS

This study is funded by the UK Natural Environment Research Council (NERC), UK National Centre for Atmospheric Science (NCAS), Australian Research Council (DP210102076) and Australian National Health and Medical Research Council (APP2000581). H.Z.S. and M.W. receive funding from the Engineering and Physical Sciences Research Council (EPSRC) via the UK Research and Innovation (UKRI) Centre for Doctoral Training in Application of Artificial Intelligence to the study of Environmental Risks (AI4ER, EP/S022961/1). H.Z.S. also gives thanks for generous support from the US Fulbright Program. P.Y. is supported by China Scholarship Council (no. 201906210065). Z.S. acknowledges support from the UKRI NERC Cambridge Climate, Life and Earth Doctoral Training Partnership (C-CLEAR DTP, NE/S007164/1). M.M.C. is sponsored by the Croucher Foundation and Cambridge Commonwealth, European and International Trust funding through a Croucher Cambridge International Scholarship. H.L. is supported by the National Natural Science Foundation of China (no. 42061130213) and the Royal Society of the United Kingdom through the Newton Advanced Fellowship (NAF/R1/201166). A.T.A. acknowledges funding from NERC (NE/P016383/1) and through the Met Office UKRI Clean Air Program. Y.G. is supported by a Career Development Fellowship of the Australian National Health and Medical Research Council (APP1163693). Special appreciation is extended to Prof. Xiao Lu (School of Atmospheric Sciences, Sun Yat-sen University) for his insightful discussion on the quality control of TOAR and CNEMC observations, and Prof. Aiyu Liu (Department of Sociology, Peking University) for her trenchant research perspectives on China's urbanization, to improve this current interdisciplinary research.

AUTHOR CONTRIBUTIONS

H.Z.S., A.T.A., and Y.G. conceived and designed the study. H.Z.S. performed analyses with data inputs from A.T.A., Z.L., H.Z., S.K., K.H., and H.L., cross-validated by X.L., H.W., P.Y., S.G., C.G., and M.X. A.T.A., Y.G., and H.S., led in-depth discussions from perspectives of atmospheric modeling, public health, and China studies, respectively. Z.S., M.Q., M.W.L.W., M.M.C., S.G., C.G., K.R.v.D., H.Z., and Y.L. enriched the discussion and examined the language. H.Z.S. and J.Z. wrote the manuscript with comprehensive supports from all authors.

DECLARATION OF INTERESTS

The authors declare no competing interests.

DATA AND CODE AVAILABILITY

Researchers can acquire the following datasets involved in this study. (1) Accesses to the four developed ambient O_3 concentration databases are stated in the original literatures, among which a public version of TAP with near-real-time updating can be retrieved at: http://tapdata.org.cn. (2) TOAR archive for global ambient O_3 *in situ* observations: https://join.fz-juelich.de/services/rest/surfacedata. (3) Processed CNEMC archive for China *in situ* observations: https://quotsoft.net/air. (4) High-resolution gridded population: https://sedac.ciesin.columbia.edu/data/collection/gpw-v4. (5) Urban-rural differentiated gridded population: https://sedac.ciesin.columbia.edu/data/collection/grump-v1. (6) Annual cause-specific baseline mortality metrics by Global Burden of Disease Mortality and Causes of Death Collaborators: http://ghdx.healthdata.org/gbd-results-tool. (7) MEIC emission inventories: http://meicmodel.org.cn. (8) Chemistry-climate interactive emission inventory of biogenic non-methane VOCs: https://esgf-node.llnl.gov/search/cmip6 (select Institution ID = "*NCAR*," Experiment ID = "*historical*" or "*ssp370*," Variable = "*emibvoc*," Variant Label = "*r1i1p1f1*"). (9) Land use information database: https://esgf-node.llnl.gov/search/input4mips (select Source ID = "*UofMD-landState-AIM-ssp370-2-1-f*" or "*UofMD-landState-high-2-1-h*," Variable = "*multiple-states*"). (10) China Statistical Yearbook 1981–2021 series: www.yearbookchina.com. The processed datasets are archived at UK Centre for Environmental Data Analysis via JASMIN supercomputer, and can be shared upon request to the corresponding author A.T.A. at ata27@cam.ac.uk. A mixture of Python (version 3.8.0), R (version 4.1.3), Stata (standard edition 17.0), and QGIS (version 3.26) was used for data processing, analysis, plotting, and geographical mapping. Demonstrative codes will be available at https://github.com/csuen27/ozone-mortality.

SUPPLEMENTAL INFORMATION

It can be found online at https://doi.org/10.1016/j.xinn.2023.100517.

LEAD CONTACT WEBSITE

Professor Alexander T. Archibald: https://www.ch.cam.ac.uk/person/ata27
Professor Yuming Guo: https://research.monash.edu/en/persons/yuming-guo
Professor Huan Liu: https://www.tsinghua.edu.cn/enven/info/1052/1978.htm